Earth and Planetary Science Letters 614 (2023) 118190

Contents lists available at ScienceDirect

Earth and Planetary Science Letters

journal homepage: www.elsevier.com/locate/epsl

Uranium isotope evidence for extensive seafloor anoxia after the end-Triassic mass extinction

Anna Somlyay [a,b,*], László Palcsu [c], Gabriella Ilona Kiss [c], Matthew O. Clarkson [d], Emma Blanka Kovács [e], Zsolt Vallner [a,c], Norbert Zajzon [f], József Pálfy [a,b]

[a] Department of Geology, Institute of Geography and Earth Sciences, Eötvös Loránd University, 1117 Budapest, Hungary
[b] ELKH-MTM-ELTE Research Group for Paleontology, 1117 Budapest, Hungary
[c] Isotope Climatology and Environmental Research Centre (ICER), Institute for Nuclear Research, 4026 Debrecen, Hungary
[d] Department of Earth Sciences, ETHZ, 8092 Zurich, Switzerland
[e] Department of Geology, and Earth Surface Research Laboratory (ESRL), Trinity College Dublin, The University of Dublin, College Green, Dublin 2, Ireland
[f] Institute of Mineralogy and Petrology, University of Miskolc, Miskolc-Egyetemváros H-3515, Hungary

ARTICLE INFO

Article history:
Received 31 August 2022
Received in revised form 14 March 2023
Accepted 22 April 2023
Available online 12 May 2023
Editor: A. Jacobson

Keywords:
Triassic-Jurassic boundary
oxygen depletion
$\delta^{238}U$
geochemical modeling
biotic recovery

ABSTRACT

The end-Triassic extinction (ETE) ranks as one of the 'Big Five' biotic crises of the Phanerozoic and is thought to be triggered by volcanism of the Central Atlantic Magmatic Province (CAMP). However, the proximal causes of the extinction and the factors responsible for the delayed biotic recovery remain debated. Here we use uranium isotopes and geochemical models to constrain the evolution of global seafloor anoxia during the latest Triassic and earliest Jurassic. We document a major negative uranium isotope anomaly from carbonates in a western Tethyan continuous marine Triassic-Jurassic boundary section. The onset of the $\delta^{238}U$ anomaly is coincident with the initial negative carbon isotope anomaly that is correlative with the extinction horizon and a major pulse of intrusive CAMP volcanism. The U isotope values remain low throughout most of the Hettangian indicating persistent, widespread anoxia. Our coupled C-P-U Earth system and U-cycle box model results show that the maximum extent of anoxia (~13%) was reached 200–250 kyr after the extinction, probably as a consequence of extrusive CAMP pulses. The anoxic extent remained high (1–6%) throughout the Hettangian. We suggest that the continuing volcanic activity, recorded by the successive negative carbon isotope anomalies and Hg peaks in the section, inhibited any rapid recovery from anoxia. Our results indicate that the spread of marine anoxia and the ETE have a common cause rather than a cause-and-effect relationship but anoxia played a key role in hindering the biotic recovery of benthic ecosystems following the extinction.

1. Introduction

The end-Triassic mass extinction (ETE) occurred 201.4 million years ago (Schoene et al., 2010) and ranks as one of the 'Big Five' biotic crises in the Phanerozoic, marked by the extinction of ~80% of the species (Sepkoski, 1996). The leading hypothesis to explain the extinction proposes that the ecosystem collapse was the consequence of environmental changes triggered by volcanism of the Central Atlantic Magmatic Province (CAMP) (Marzoli et al., 2004). The duration of the main CAMP volcanism was ~850 kyr (Schaller et al., 2011), however, the volcanic activity continued for several million years (Marzoli et al., 2019). The cause-and-effect relationship is suggested by the synchrony of the extinction horizon with a carbon isotope anomaly in several Triassic-Jurassic boundary (TJB) sections (Hesselbo et al., 2002; Korte et al., 2019). This large and rapid negative initial carbon isotope excursion (ICIE) is linked to the onset of CAMP activity (Davies et al., 2017; McElwain et al., 1999; Pálfy et al., 2001). However, the proximal trigger mechanisms for the ETE remain debated. The proposed main drivers include lethally elevated temperatures (McElwain et al., 1999; Schaller et al., 2011), ocean acidification (Greene et al., 2012), and anoxia (Hallam, 1995; Jost et al., 2017b; Wignall and Atkinson, 2020). Oxygen-depleted conditions during the boundary interval are recorded by widespread black shale deposition and were inferred in previous studies from local paleoredox proxies (Hallam, 1995), $\delta^{238}U$ anomaly (Jost et al., 2017b), $\delta^{34}S_{CAS}$ anomaly (He et al., 2020), and biomarker data (Richoz et al., 2012; van de Schootbrugge et al., 2013).

* Corresponding author at: Department of Geology, Institute of Geography and Earth Sciences, Eötvös Loránd University, 1117 Budapest, Hungary.
E-mail address: anna.somlyay@erdw.ethz.ch (A. Somlyay).

https://doi.org/10.1016/j.epsl.2023.118190

The uranium isotope ratio ($^{238}U/^{235}U$, expressed as $\delta^{238}U$) in marine carbonates is an established proxy for reconstructing the extent and temporal evolution of seafloor anoxia in ancient oceans. Uranium is strongly redox-sensitive, with the reduction of U(VI) to U(IV) predominantly occurring within anoxic sediments. The reduced, insoluble uranium favors ^{238}U, leaving the soluble U(VI) in the water column preferentially enriched in ^{235}U (Andersen et al., 2014; Weyer et al., 2008). Since the residence time of uranium is ~450–500 kyr in the modern ocean (Dunk et al., 2002), significantly longer than the mixing time of seawater (~1–2 kyr), the uranium isotopic composition is homogeneous in the world ocean (Weyer et al., 2008). Consequently, variations of seawater U isotopic ratios can reflect the changes in the redox conditions of the oceans at a global scale. Since primary calcium carbonates can directly record seawater $\delta^{238}U$ with negligible isotope fractionations (<0.1 per mil; Chen et al., 2018a; Livermore et al., 2020), the U isotope signature preserved in limestones can serve as a global proxy for the areal extent of anoxic sediment at the time of their deposition (Zhang et al., 2020). Indeed, negative $\delta^{238}U$ excursions have been identified for several mass extinction and deoxygenation events (Lau et al., 2016; Jost et al., 2017b; Bartlett et al., 2018; Clarkson et al., 2018; Zhang et al., 2018). The global reproducibility of $\delta^{238}U$ signals has been confirmed by some studies, in particular for the end-Permian mass extinction (Brennecka et al., 2010; Lau et al., 2016; Zhang et al., 2018), which is important for identifying the true magnitude and timing of $\delta^{238}U$ changes in light of possibly significant diagenetic modification of $\delta^{238}U$ in marine carbonates that tend to increase $\delta^{238}U$ (Romaniello et al., 2013; Chen et al., 2018a, 2021, 2022; Tissot et al., 2018). For the Triassic-Jurassic boundary interval, so far only one study reported a negative $\delta^{238}U$ excursion from two closely located sections in the Lombardy Basin in Italy (Jost et al., 2017b) but no attempt has yet been made to replicate this result and to explore extended Late Triassic baseline values.

Here we present a new $\delta^{238}U$ dataset from a Triassic-Jurassic boundary section at Csővár (Transdanubian Range, Hungary) which was among the first localities worldwide where the TJB event was recognized in the carbon isotope record (Pálfy et al., 2001). The available multiproxy geochemical data include recently generated high-resolution carbon isotope and mercury concentration data (Kovács et al., 2020). The joint assessment of the uranium cycle with that of carbon and mercury gives new insights into the Earth system processes and the possible causes of anoxia.

Using the input of geochemical datasets, we also present a dynamic uranium cycle box model and a coupled C-P-U model to develop a quantitative reconstruction of seafloor redox conditions and characterize the response of carbon, phosphorus, and uranium cycles to volcanic CO_2 degassing. The interpretation of the geochemical data and model results helps to elucidate the role of anoxia in triggering the marine ETE and hindering the subsequent biotic recovery.

2. Geological setting

The Csővár section exposed on Vár-hegy ("Castle Hill") is located 45 km north-northeast of Budapest, near the village of Csővár, east of the Danube River. The predominantly limestone succession is exposed in outcrops that constitute the northeastern termination of the Transdanubian Range. In the tectonostratigraphic sense, it is part of the Alcapa Unit (Haas et al., 2010). The study area lies within the fault-bounded, uplifted Nézsa-Csővár block (Pálfy et al., 2001, 2007). The carbonates were deposited in an intraplatform basin in slope, toe-of-slope, and basinal environments (Haas et al., 2010). The water column was thought to be well-oxygenated as indicated by the low Mn and V content (Vallner et al., 2023) and the presence of benthic micro- and macrofossils (Pálfy et al., 2007). Thus uranium isotopes measured from carbonates ($\delta^{238}U_{carb}$) is expected to faithfully record the value of the contemporaneous world ocean ($\delta^{238}U_{sw}$). The studied succession is assigned to the Csővár Limestone Formation and the sampled interval was deposited between the late Rhaetian and late Hettangian, representing 2.9–3 Myr based on an astrochronological age model, 1.08–1.21 Myr assigned for the Rhaetian and 1.73–1.81 Myr for the Hettangian, respectively, supporting a short (~2 Myr) duration for the entire Hettangian stage (Vallner et al., 2023). The Csővár section is well-suited for geochemical analyses for its homogenous lithology and continuous deposition across the TJB, constrained by ammonoid, conodont, radiolarian, and foraminiferan biostratigraphy (Pálfy et al., 2001, 2007) (for details, see the Supplementary material).

3. Material and methods

The sample preparation and the geochemical analyses were carried out at the Isotope Climatology and Environmental Research Center at Institute for Nuclear Research (ATOMKI) in Debrecen, Hungary. Twenty-eight limestone samples were powdered and 1 g of fresh rock powder from each sample was digested in 2% twice distilled HCl overnight. The supernatants containing the carbonate fraction were separated from the undissolved residues and were filtered and evaporated. Subsequently, a 2000-fold diluted IRMM 3636a spike was added to each sample to obtain a ^{235}U:^{233}U sample to spike ratio of ~2:3. Uranium was isolated and purified via column chemistry using the UTEVA ion exchange resin following the procedures adapted from Weyer et al. (2008). The uranium-enriched samples were treated with cc. HNO_3 and evaporated, then dissolved in 2 ml 3% HNO_3 for uranium isotope analysis. For a summary of the preparation steps, see Table S1 (Supplementary material).

$\delta^{238}U$ measurements were performed using a Thermo Scientific™ NEPTUNE Plus™ MC-ICP-MS. Results were calibrated using the international standard synthetic reference material CRM 112A. Each sample has been measured a minimum of three times with standard–sample bracketing. Analytical errors of measurements range from 0.02‰ to 0.12‰ ($\pm 1\sigma$) which is consistent with the analytical errors of previously published uranium isotope data. To assess the external reproducibility, we measured modern seawater samples with reported uranium isotope values (Table S3, Andersen et al., 2017). These samples underwent column chemistry in the same manner as the limestone samples. The modern seawater standard gave a mean $\delta^{238}U$ value of -0.409 ± 0.029‰ (1 SD) which is in agreement with the previously published value -0.39 ± 0.01‰ (2 SD, Andersen et al., 2017).

U, Th, Al, Mn, Sr, Mg, and Ca concentrations were measured using an Agilent 8800 Triple Quad ICP-MS. A full description of the sample preparation procedure and analytical methods is included in the Supplementary material. The analytical data from this study are also presented in the Supplementary material.

4. Results

The Csővár section yielded uranium isotopic values ranging from −0.94‰ to 0.26‰ (Fig. 1, Table S3). In the lower part of the section, $\delta^{238}U$ oscillates around an average value of 0.077‰. At 17.6 m, in the interval also marked by the ICIE, $\delta^{238}U$ declines abruptly from −0.39‰ to −0.63‰. The decreasing trend continues towards the TJB with a minimum value of −0.94‰ at 20.8 m, c. 240 kyrs after the onset of the uranium isotope anomaly. The age estimate is based on the astrochronological age model of the section (Vallner et al., 2023). The negative $\delta^{238}U$ excursion observed in the lower part of the section continues through the TJB

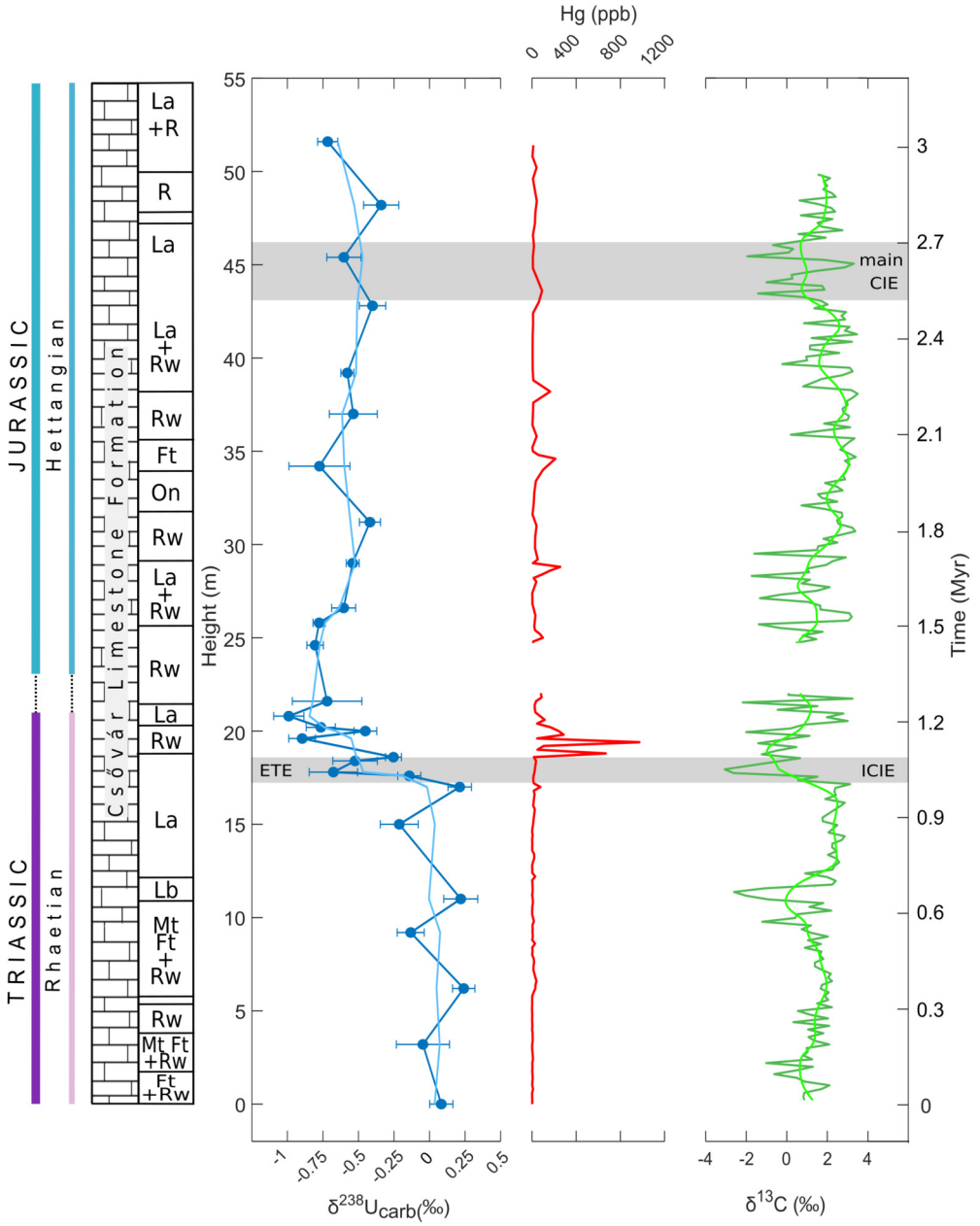

Fig. 1. Uranium isotope, mercury (Kovács et al., 2020), and carbon isotope data (Kovács et al., 2020) from the Csővár section. LOESS smoothed curves are shown for uranium (in light blue, f=0.06) and carbon isotopes (Kovács et al., 2020) (in light green, f=0.1). The lower gray band marks the ICIE and the extinction, the upper gray band highlights one of the subsequent Hettangian carbon isotope anomalies (NCIE-5 in Kovács et al., 2020). The astrochronological age model is from Vallner et al. (2023), lithostratigraphy and carbonate microfacies log from Haas and Tardy-Filácz (2004). Rw: radiolarian wackestone, La: calcisiltite-calcilutite laminate, Ft: fine-grained turbidite, Mt: medium-grained turbidite, Lb: lithoclastic-bioclastic grainstone/packstone, On: oncoid, grapestone/packstone/wackestone. The uranium isotope record covers the entire section representing 1–1.2 Myr for the Rhaetian, and 1.7–1.8 Myr for the Hettangian (early to late Hettangian). The Hg content already starts to increase at the onset of the carbon and uranium isotope anomaly (10-fold increase) before reaching its maximum value (more than 100-fold increase above 18.5 m).

interval. Higher upsection, $\delta^{238}U$ values do not return to the pre-anomaly background but remain low (average of −0.54‰) and steady throughout the Hettangian.

The uranium concentrations are relatively high (average of 3 ppm) at the base of the section (Table S3), but similar to primary shallow water carbonates Romaniello et al., (2013). The samples from the lowermost 9.2 m yielded the three highest [U] values in the section (Fig. 1, Table S3). After a decrease from 3.063 to 1.483 ppm (0–3.2 m) the values show a clear increasing trend up to 9.2 m where they reach the peak value of 5.129 ppm followed by an abrupt drop to 0.868 ppm at 11 m. Above 11 m the values remain low throughout the section. Up to 17 m there is a slight increase toward higher values, the concentration of 2.099 ppm measured at 17 m represents the highest value above 9.2 m. After that, the U concentration abruptly decreases to 0.413 ppm. Between 17.6–21.6 m the values remain low and fluctuate with relatively high amplitude showing no clear trend. The lowest value of the section occurs in this interval (0.317 ppm at 21.6 m). Above 24.6 m up to the uppermost part of the section the U concentrations do not increase towards higher values, the samples from this interval yielded an average value of 0.867 ppm with a local maximum of 1.803 ppm at 34.2 m. Moreover, the data points do not show any significant oscillation.

We also analyzed the Th, Al, Mn, Sr, Mg, and Ca content to evaluate the potential effect of diagenesis and terrestrial input on $\delta^{238}U$. The concentrations of these elements do not show signifi-

cant variation across the section and their magnitudes are similar to those of other marine limestones (Fig. S1, Table S3).

5. Discussion

5.1. Effects of diagenesis and local redox conditions on preservation of seawater $\delta^{238}U$ signal

The $\delta^{238}U_{carb}$ of the Csővár section likely represents the $\delta^{238}U_{sw}$. The most important evidence for this is the similarity of its uranium isotope data to those of the Lombardian Triassic-Jurassic boundary sections (Jost et al., 2017b). In all the three TJB sections a negative uranium isotope anomaly was detected at the stratigraphic position of the initial CIE below the TJB indicating a global $\delta^{238}U$ signal (Fig. 3). $\delta^{238}U_{carb}$ remains low in the Lower Jurassic parts of the sections. The uranium isotope data of Csővár and the Lombardian sections are compared in detail later in this section.

Uranium isotope ratios are sensitive to diagenesis (Romaniello et al., 2013; Chen et al., 2018a, 2018b; Hood et al., 2016; Tissot et al., 2018; Chen et al., 2022). Therefore, we performed geochemical tests to assess the degree of diagenetic alteration in the studied samples. Excluding a single outlier at 21 m, the samples yielded an average $\delta^{18}O$ value of −2.57‰ (Table S3), hence the effect of meteoric diagenesis was probably not significant based on the oxygen isotope ratios. Similarly, the Mn/Sr ratios that range between 0.015–0.128 (Table S3) are well below the proposed maximum acceptable ratio of 2 (Brand, 2004). The correlation of $\delta^{238}U$ with Mn/Sr, Mn/Ca, and Sr/Ca is weak, −0.08, −0.05, and 0.05, respectively (Fig. S2). The Val Adrara and Italcementi sections in Lombardy that yielded the first uranium isotope data across the TJB (Jost et al., 2017b) have similar oxygen isotope values and Mn/Sr ratios to those in the Csővár section. Importantly, however, the traditional geochemical tools for screening diagenetic alterations are not sufficient to exclude potential alterations in the original uranium isotope signal.

The $\delta^{238}U$ values in the lower part of the section are significantly higher than the uranium isotope composition of modern seawater (−0.39 ± 0.01‰) (Weyer et al., 2008). These positive values are in agreement with the previously published uranium isotope data of shallow marine carbonates and were also observed in modern platform carbonate settings (Romaniello et al., 2013; Chen et al., 2018a). The positive offset is likely developed during early diagenesis as a result of the incorporation of reduced U with a heavier isotopic ratio. In general, shallow marine settings tend to produce greater diagenetic offsets than pelagic environments which appear to record the original $\delta^{238}U$ signal more directly (Clarkson et al., 2018). However, the shallow marine Val Adrara-Italcementi sections have baseline isotopic values closer to the seawater, probably indicating a greater degree of diagenesis in the uppermost Triassic part of the Csővár section. Therefore, we applied a diagenetic correction factor of −0.27‰ based on the average observed offset between seawater and modern carbonate sediments (Romaniello et al., 2013; Tissot and Dauphas, 2015; Chen et al., 2018a) (Fig. S3). Some of the corrected isotopic values are still higher than the $\delta^{238}U$ of the modern ocean, that can be explained by the high degree of scatter observed due to diagenesis (±0.14, 1σ; Chen et al., 2018a).

A plausible explanation for the anomalously high uranium isotope values of the section is the addition of calcitic cement enriched in heavier uranium during diagenesis (Chen et al., 2022). The carbonates of the Csővár section have a primary calcitic mineralogy that preserves the $\delta^{238}U$ signal with a larger positive offset compared to aragonite. Aragonite contains an order of magnitude more uranium compared to calcite (>1 ppm vs. <0.1 ppm), consequently, the effect of heavy uranium produced by porewater U reduction during diagenesis is smaller (Chen et al., 2022). The U concentration of the Csővár section is higher than that of primary calcite (>0.4 ppm vs. <100 ppb) indicating authigenic U(IV) incorporation. The accumulation of U(IV) in reducing porewater below the sediment-water interface can cause an isotopic offset of up to 0.59‰ (Chen et al., 2022), which may explain the observed offset of +0.46‰ between $\delta^{238}U_{carb}$ and $\delta^{238}U_{sw}$ in the lower (pre-anomaly) part of the Csővár section (Fig. 1). We evaluated the potential impact of the detrital component of terrestrial U input on the $\delta^{238}U_{carb}$ and U concentration trends by comparing [U] and $\delta^{238}U$ to concentrations of Al and Th (Table S3). The weak correlations support the independence of the major changes in $\delta^{238}U$ from weathering processes.

The evolution of $\delta^{238}U$ tracks the global redox conditions reliably only if measured in sedimentary rocks deposited in oxic waters (Clarkson et al., 2021; Chen et al., 2021) which can preserve the uranium isotope ratio with only negligible fractionation. To exclude the possibility that potentially hypoxic bottom waters in the Csővár basin resulted in $\delta^{238}U$ values not representative of the world ocean, local paleoredox proxies were also utilized. The low whole-rock V (<0.18%) and Mn (<0.46%) content within the section (Vallner et al., 2023) indicate an oxic local depositional environment. The abundance of Ce shows opposite trends compared to other redox-sensitive elements during redox-state changes (Tostevin, 2021). Anoxic sediments do not produce Ce anomalies whereas negative Ce anomalies of the carbonate fraction reflect oxygenated water during deposition. Importantly, Ce/Ce* does not give information on the redox conditions below the sediment-water interface. Carbonates deposited in oxic water but affected by reduced porewaters may show negative Ce anomaly as well (e.g. Csővár section and PETM carbonates from ODP Hole 871C, Chen et al., 2022). The negative Ce/Ce* anomaly (Ce/Ce* ratios: 0.48–0.74) of the broader TJB interval indicate stable, well-oxygenated local bottom-water conditions in the Csővár basin throughout the major negative shift of $\delta^{238}U$ (Fig. 2, Table S3).

5.2. Comparison of the $\delta^{238}U$ trends in Csővár and the Lombardian sections

In the first study published that reports $\delta^{238}U$ data from the TJB interval (Jost et al., 2017b), uranium isotope data were obtained from the Val Adrara and Italcementi sections that were deposited in the Lombardy Basin, located in the Italian Alps. The correlation between the Csővár section and those in Lombardy is hampered by the application of different stratigraphic methods that yielded partly contradictory age models. For the Csővár section, the time of deposition (2.9–3 Myr), the sedimentation rates (1.73–1.79 cm/kyr), the position of the TJB (~22 m), and the duration of the initial carbon isotope anomaly (~40–80 kyr) are well-constrained (Vallner et al., 2023). The age model is based on astrochronology and chronostratigraphic correlation developed using congruent biostratigraphy of different fossil groups (ammonoids, conodont, radiolarians, palynomorphs) and carbon isotope stratigraphy (Kovács et al., 2020; Pálfy et al., 2001, 2007; Vallner et al., 2023) (see Supplementary material). On the other hand, no cyclostratigraphic analysis is available for the Val Adrara and Italcementi sections that prevents astrochronological correlation. Magnetostratigraphy is available from the Italian sections (Muttoni et al., 2010), however, the paleomagnetic signal of the Csővár section is overprinted (Pálfy et al., 2007). The large (~4‰) positive carbon isotope anomaly in the Val Adrara section detected above the boundary is confined to the oolitic dolomite of the Albenza Fm. (van de Schootbrugge et al., 2008) and was not reproduced in most other TJB localities including Csővár, hence it cannot be used for precise correlation of these sections (Korte et al., 2019).

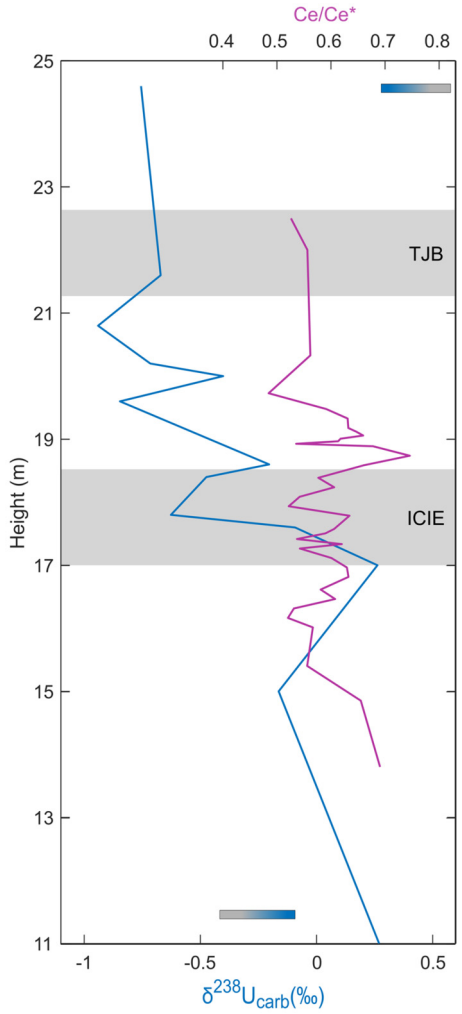

Fig. 2. Uranium isotope and Ce/Ce* data from the TJB interval of the Csővár section. Low Ce/Ce* values (<0.9, Sholkovitz et al., 1994) indicate well-oxygenated local redox conditions. Higher Ce/Ce* values indicate less oxygenated local redox conditions as it is illustrated in the upper colored bar (blue to gray – oxygenated to less oxygenated local bottom waters). Negative δ^{238}U values ($<\delta^{238}U_{SW}$=0.39‰, Weyer et al., 2008, gray part of the lower colored bar) indicate an increased extent of global seafloor anoxia. The position of the TJB and the ICIE is marked by gray shade, based on the combination of carbon isotope- and cyclostratigraphy (Kovács et al., 2020; Vallner et al., 2023).

The frames of reference to correlate the sections include the position of the TJB and the negative uranium and carbon isotope anomalies, of which the ICIE is of prime importance (Galli et al., 2007). Besides the ICIE, the other NCIEs and age models are used here to compare the three sections. We present two different solutions for the correlation, one that relies on published carbon cycle modeling results (Bachan and Payne, 2015) (Fig. 3A) and our preferred alternative that utilizes sedimentation rate estimates for the Val Adrara section and is validated by biostratigraphy (Fig. 3B). Based on the carbon cycle model results and their correlation with the NCIEs of the Val Adrara section, the upper part of the section that lies above the ETE interval would represent 620 and 840 kyr, respectively, of which the latter was used in interpreting the U data (Jost et al., 2017b). If this were the case, the Hettangian segment of δ^{238}U data from Csővár (representing ~1.8 Myr) (Vallner et al., 2023) represents approximately twice as much time as that from the Val Adrara section (Fig. 3A). We propose an alternative correlation (Fig. 3B) based on sedimentation rate estimates for the Albenza Formation of the Val Adrara section (Jadoul and Galli, 2008). A sedimentation rate of 125 m/Myr was calculated for the Albenza Formation, suggesting that the Sedrina Formation extends into the upper Hettangian. This indicates a ~1.9 Myr interval of deposition and implies that the Hettangian uranium isotope data of the Csővár and Val Adrara sections represent approximately the same time (Fig. 3B). The well-preserved ammonoids identified as *Schlotheimia* sp. from the upper part of the Sedrina Formation are assigned to the base of the upper Hettangian Angulata Zone (Gaetani, 1970). The occurrence of *Schlotheimia* sp. also near the top of the Csővár section (Kovács et al., 2020) supports an approximate biostratigraphic correlation between the top of the two sections compared here. Note that independent of these correlation options, the decrease of the δ^{238}U values coincides with a major negative carbon isotope anomaly, identified as the ICIE in both sections (Galli et al., 2007; Kovács et al., 2020; Pálfy et al., 2007) (Fig. 3).

Although the Csővár, Val Adrara, and Italcementi sections yield congruent δ^{238}U trends, a difference in the magnitude of the negative δ^{238}U anomaly is observed, and the isotopic values of the Csővár section are systematically lower than that of the Val Adrara section throughout the Hettangian. We note that a diagenetic correction factor of −0.27‰ has been applied for the δ^{238}U curve of Csővár, whereas the δ^{238}U values of the Val Adrara and Italcementi sections were not corrected. If the diagenetic correction factor is applied for the Lombardian sections, the δ^{238}U curve reaches a minimum of −0.96‰ which is still higher than the corrected minimum value of the Csővár section (−1.11‰). Moreover, regardless of the application of the diagenetic correction factor, a more significant relative drop (~-0.75‰) from the Rhaetian baseline δ^{238}U characterizes the Csővár section compared to the Val Adrara-Italcementi sections (~-0.5‰). This discrepancy is probably caused by different magnitudes of diagenesis in the Lombardy and Csővár basins. The difference may be accounted for by the facies changes of the Lombardian sections, albeit the processes leading to disparate δ^{238}U in different depositional settings are poorly known. Importantly, there are no significant facies changes in the TJB interval of the Csővár section. However, in the Lombardian sections, the onset of the uranium isotope anomaly approximately coincides with the boundary between the Zu and Malanotte formations that marks a change in sedimentation and represents a major lithofacies change from coralline packstone to thin-bedded marly mudstone (Galli et al., 2005; Jost et al., 2017b, Fig. 3). However, in general, δ^{238}U is considered as largely independent of facies changes, as long as the depositional environment remains oxic, hence the magnitude difference is unlikely to be the result of facies changes in the Lombardian sections.

Another possible reason for the offset in the uranium isotopic values of the sections is the geographical variability in U speciation as a consequence of the altered seawater carbonate chemistry at times of environmental perturbations (Chen et al., 2017). Based on laboratory experiment results (Chen et al., 2016), in contrast to uncharged species, charged U species favor the light uranium isotopes. However, the spatial variability of U speciation in the late Triassic ocean is poorly constrained. Variable U speciation is proposed to have led to heterogenous uranium isotope values across the Permian-Triassic boundary interval (Chen et al., 2017; Lau et al., 2016). More acidic pH and higher seawater [Ca^{2+}] result in a greater offset between the $\delta^{238}U_{seawater}$ and $\delta^{238}U_{carb}$. The changing seawater chemistry and the altered U speciation may cause fractionation up to +0.18‰ (Chen et al., 2017), so it would only partially explain the observed magnitude difference of the uranium isotope anomalies. The prevalence of aragonite mineralogy in a brief interval above the TJB in the Val Adrara section suggests transitional seawater chemistry after ocean acidification (Jost et al., 2017a, 2017b). Similarly to anoxia, ocean acidification may have been induced by the CAMP volcanism and was proposed as a trigger of the ETE (Kiessling et al., 2010). The recovery from the

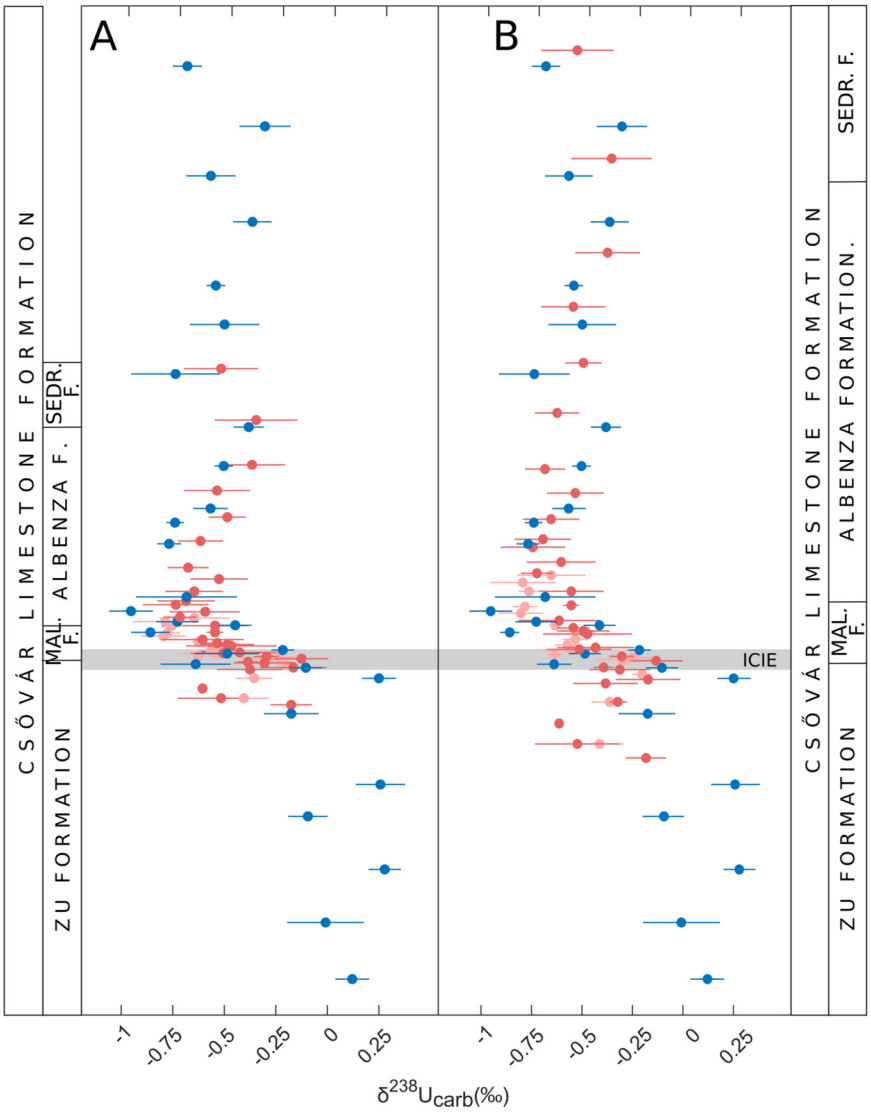

Fig. 3. Comparison of measured U isotope data from the Csővár section (this study) with the Val Adrara and Italcementi sections in Lombardy (Jost et al., 2017b) using alternative solutions for correlation. (*A*) Correlation in Jost et al. (2017b) based on carbon cycle model results (Bachan and Payne, 2015) (B) Our preferred correlation is based on sedimentation rate estimates (Jadoul and Galli, 2008). The blue dots represent the Csővár section, the red and light red dots represent the Val Adrara and Italcementi sections, respectively. As the measured baseline values are negative, no diagenetic correction factor was applied for the Lombardian sections (Jost et al., 2017b). The horizontal gray bar marks the ICIE identified in both sections. F.: Formation, Mal.: Malanotte, Sedr.: Sedrino. See text for details.

acidification is marked by the prevalence of aragonite mineralogy in the Lombardian sections. This change has not been observed in the limestones of the Csővár section where calcite mineralogy is predominant. The changing seawater pH indicated by the calcite-aragonite transition in the Lombardy Basin might have slightly influenced the uranium isotope fractionation (up to 0.18‰, Chen et al., 2016). The transition from calcite to aragonite mineralogy itself is probably also significant in altering the $\delta^{238}U_{sw}$ preservation.

The mineralogy change affected the $\delta^{44/40}Ca$ values of the Lombardian sections and it might have also altered the magnitude of uranium isotope offset. Aragonite is shown to perverse the original uranium isotope signal with a smaller positive offset compared to calcite (Chen et al., 2022). Consequently, immediately above the TJB, the uranium isotope values should be more negative in the Lombardian sections where the mineralogy is aragonitic compared to the Csővár section where the mineralogy remains calcitic. In contrast, the $\delta^{238}U_{carb}$ values of this part of the Csővár section are lower and the negative shift is larger. Hence the observed difference in the magnitude of the negative anomaly cannot be caused by the different effect of authigenic U incorporation into calcite vs. aragonite on the original $\delta^{238}U$ signal.

Aragonites are proposed to preferentially incorporate heavier uranium isotopes at pH 8.5 (Chen et al., 2016). This can partially explain the heavier uranium isotope ratios of the Val Adrara-Italcementi sections compared to the Csővár section, but it is not yet supported by sufficient data or observations.

It is possible that the combination of the above mentioned factors led to altered uranium isotope signals, but available evidence for each hypothesis is limited and further research is needed to constrain the influence of the seawater chemistry on the $\delta^{238}U_{carb}$ and the magnitude of fractionation.

5.3. Modeling the expansion of anoxia as a consequence of CAMP pulses

The major $\delta^{238}U$ decline from −0.39‰ to −0.93‰ in the Csővár section at 17.6 m (Fig. 3) suggests a rapid increase in the global extent of seafloor anoxia. The beginning of the negative uranium isotope excursion corresponds with the negative $\delta^{13}C$ excursion at 17–18.4 m which is the most prominent $\delta^{13}C$ anomaly

of the section identified as the ICIE and with a minor increase in the Hg content (Kovács et al., 2020) (Fig. 1, Table S3). The carbon isotope anomaly is thought to be associated either with thermogenic methane release related to the intrusive CAMP activity and metamorphism of organic-rich country rock (Davies et al., 2017; Heimdal et al., 2020) or with warming-induced methane-hydrate dissociation (Pálfy et al., 2001). The limited enrichment in Hg seen concomitantly in the Csővár section is consistent with a predominantly intrusive initial phase of volcanism. By contrast, the onset of extrusive CAMP volcanism is marked by the most significant Hg peak at 19.4 m and episodic enrichments higher in the section (Kovács et al., 2020) (Fig. 1). The concurrent drop of $\delta^{13}C$ and $\delta^{238}U$ indicates a coeval global perturbation of the carbon and uranium cycles, suggesting a cause-and-effect relationship between CAMP activity and marine anoxia. As the ICIE coincides with the extinction horizon (Korte et al., 2019; Ruhl et al., 2009), the global redox state change of the ocean appears nearly synchronous with the collapse of the marine ecosystem at the end of the Rhaetian. However, the interpretation of the $\delta^{238}U$ values is not entirely straightforward. The uranium system has a delayed response time to the changes in the areal extent of the seafloor anoxia because of the long residence time of the element (~490–500 kyr). Hence, the samples yielding the most negative values do not strictly represent times with the most severe anoxic conditions and the duration of the uranium isotope anomaly might be longer than the duration of the anoxic event. To account for the delayed response time of uranium and to quantify the extent of the marine anoxia and its temporal evolution we applied a dynamic Earth system model.

The C-P-U model (Clarkson et al., 2018), which is derived from the COPSE model (Lenton et al., 2018), links the carbon, phosphorus, and uranium cycles. In cases when environmental perturbations (including anoxia) are induced by CO_2 injections, the coupled modeling of carbon, phosphorus, and uranium cycles provides valuable insight into the feedback mechanisms of the Earth system (for the model equations, see Supplementary material, whereas a full model description is given in Clarkson et al., 2018.) In the model, elevated atmospheric CO_2 levels lead to global warming and high weathering rates. Intense weathering at the end of the Rhaetian is indicated by observed shifts in strontium and osmium isotope ratios (Cohen and Coe, 2007). Enhanced silicate weathering acts as the long term sink for atmospheric carbon and, on shorter timescales, results in enhanced riverine P (and U) input into the ocean. The increased availability of P in surface waters promotes high primary productivity and enhanced marine organic carbon burial, that in turn induces marine anoxia via the greater oxygen demand required for organic matter decay. The recycling of phosphorus from anoxic sediments induces a positive feedback loop by further stimulating primary productivity. Under anoxic and euxinic seafloor conditions, both the organic carbon and uranium burial rates increase, removing isotopically lighter carbon and heavier uranium from the seawater. The model tracks relative changes in the seawater uranium inventory and isotopes, allowing the estimation of the history of redox state changes in the ocean responsible for the observed [U] and $\delta^{238}U$ pattern.

The model was set up for Late Triassic background conditions (see Supplementary material), with atmospheric pO_2 estimated as equal to modern. Model scenarios tested different fractionation factor estimates to account for the variable magnitude of U isotope fractionation into anoxic sediments under predominantly diffusion-limited reduction regimes (Andersen et al., 2014). As commonly used in other studies (e.g. Clarkson et al., 2021; Zhang et al., 2020) the effective U enrichment factor (Δ_{anox}) was set to +0.4, +0.6, and +0.8‰ (Fig. 4F), covering the range of values observed in modern euxinic basins (Andersen et al., 2014; Noordmann et al., 2015; Rolison et al., 2017).

The model was forced by episodic carbon emissions, where emission scenarios were tuned to produce good agreement between the $\delta^{13}C$ and $\delta^{238}U$ records. Essentially the magnitude of emission dictates the total seafloor anoxia response and hence decreases in $\delta^{238}U$. The $\delta^{13}C$ value of the carbon input ($\delta^{13}C_{input}$) is then treated as a free parameter and tuned to help meet the constraints of the two records. In this way, the $\delta^{13}C$ record helps diagnose the source of the carbon, identifying the mixture of mantle derived carbon (−5‰) and isotopically lighter thermogenic methane (Fig. 4B). The nature of CAMP volcanism was pulsatory with an initial intrusive and a delayed major extrusive phase in the late Rhaetian and early Hettangian, followed by less intense volcanic phases in the Hettangian (Davies et al., 2017; Marzoli et al., 2019; Percival et al., 2017). The pulsatory behavior is indicated by the distinct Hg peaks and negative carbon isotope anomalies detected from TJB sections (Thibodeau et al., 2016; Percival et al., 2017; Lindström et al., 2019; Ruhl et al., 2020; Kovács et al., 2020). Uncertainty remains, however, in the global significance and correlation of subsequent NCIEs after the ICIE (Kovács et al., 2020). In the Csővár section, NCIE-5 might correspond to the so-called 'main' NCIE seen elsewhere (Ruhl et al., 2009). As such we do not use NCIE-2–4 as model targets, but explore the possibility that NCIE-5 is a global anomaly.

Our model results indicate that the first, intrusive CAMP phase is responsible for the highest carbon emission magnitude (2.6×10^{14} molC), generating the main negative $\delta^{238}U$ excursion. This emission requires a $\delta^{13}C_{input}$ as low as −20‰ to reproduce the ICIE (Fig. 4A,B) consistent with previous suggestions that intrusive volcanism metamorphosed organic-rich country rocks and global warming may have driven the dissociation of methane hydrates (Ward et al., 2001; Pálfy et al., 2001). The elevated Hg content of the layers marking the intrusive CAMP phase indicates a smaller scale of extrusive volcanism accompanied the mainly intrusive volcanism.

This single LIP pulse is not able to reproduce the measured prolonged $\delta^{238}U$ and [U] excursions. Such a scenario would result in a significantly shorter uranium isotope excursion as the system quickly recovers. The $\delta^{238}U$ and U concentration of the seawater reflects the balance between U removal to anoxic and oxic sediments and U delivery from the rivers. When anoxia is widespread, U is intensely removed from the seawater to the anoxic sediments leaving the water column depleted in uranium. The small amount of U remaining in the ocean has low $\delta^{238}U$ (below −1‰ according to our modeling) because ^{238}U is preferentially removed into the anoxic sediments. However, the amount of U arriving to the ocean does not change (or even increases if the weathering intensifies) and riverine U has a constant less negative $\delta^{238}U$. Consequently, as U becomes depleted in the seawater due to the intense removal to the anoxic sediments, the inflowing 'less negative' riverine U becomes increasingly proportional in the U-depleted ocean and pushes the $\delta^{238}U_{SW}$ back towards more positive values. Because of these U-cycle dynamics, low $\delta^{238}U_{SW}$ cannot be sustained after a single C cycle perturbation. Instead, the prolonged negative uranium isotope excursion can be sustained by repeated expansion of marine anoxia as a consequence of recurrent pulses of volcanic activity. We use the Hg peaks to constrain the timing of later extrusive volcanism episodes in the model assuming predominantly mantle derived C ($\delta^{13}C_{input} = -5‰$). With repeated volcanic emissions, the marine uranium inventory only partially recovers between the anoxic phases allowing $\delta^{238}U_{sw}$ to remain steadily low. Our model results suggest that the later extrusive phases produced less amount of volcanic carbon with a maximum total emission magnitude of 1×10^{14} molC/year during the first major extrusive phase (Fig. 4A) but lasted longer than the intrusive phase. Interestingly, if NCIE-5 is used as a model target, assuming it is global in nature, the model requires this emission phase to

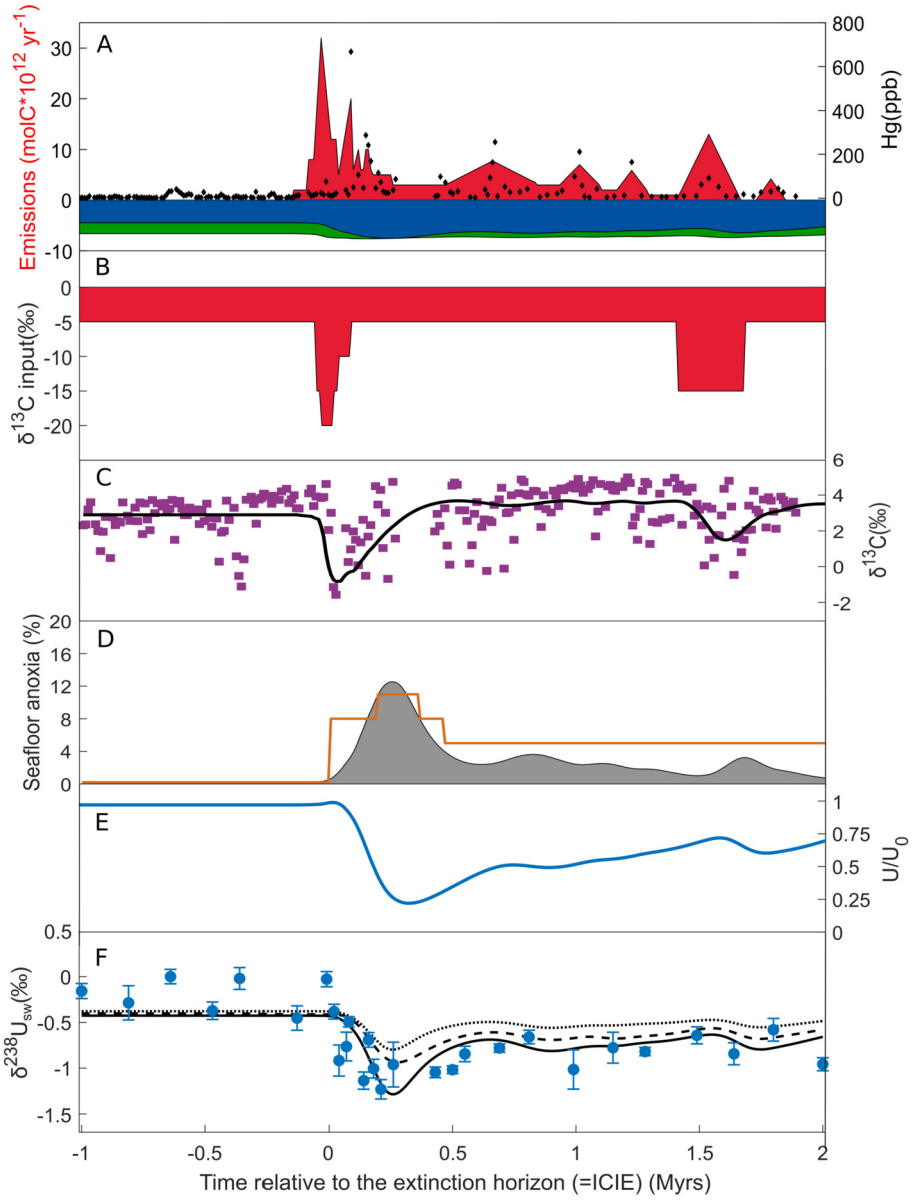

Fig. 4. Modeling of anoxia as a consequence of CAMP volcanism. The changes are given relative to the onset of the initial CIE (Vallner et al., 2023) which coincides with the main phase of the extinction. (*A*) Estimated model forcing carbon input (red peaks), estimates are based on the Hg data of the Csővár section (black dots, Kovács et al., 2020); calculated removal rates due to silicate weathering (green) and marine organic carbon burial (blue). (*B*) Estimated $\delta^{13}C$ composition of carbon input. (*C*) Modeled $\delta^{13}C$ curve (black solid line) compared to the carbon isotope data of the section (purple dots, (Kovács et al., 2020)). (*D*) Estimated extent of seafloor anoxia based on the C-P-U model (gray) and U-cycle box model (orange line). (*E*) Calculated response of marine U-cycle normalized to the U concentration of the modern ocean (U_0). (*F*) Modeled evolution of $\delta^{238}U_{sw}$ for pO_2 =1 PAL using $\Delta^{238}U_{anox}$= +0.8 (solid line), $\Delta^{238}U_{anox}$ = +0.6 (long-dashed line) and $\Delta^{238}U_{anox}$ = +0.4 (dashed line) compared to the uranium isotope data of the section (blue dots).

have a greater contribution of more isotopically light carbon, with an average of −15‰. This finding therefore hypothesizes a later, more minor intrusive phase of volcanism associated with the liberation of thermogenic methane.

Based on the C-P-U model calculations, only 1–3% of the seafloor was covered by anoxic sediments during the main extinction phase at the ICIE, which nevertheless indicates a ∼10-fold increase in the extent of the seafloor anoxia at the end of the Triassic compared to the modern steady-state value (0.21%, Andersen et al., 2014). Due to the longer residence time of P in the ocean (∼40 kyrs) and the action of positive feedback mechanisms from P recycling, peak anoxia was reached about 200–250 kyr after the extinction, when c. 13% of the global ocean floor was depleted in oxygen, representing a 60-fold increase. The C-P-U model suggests that the extent of anoxia remained elevated (0.7–1.5%) as long as ∼1.9 Myr after the onset of environmental perturbations.

We also performed dynamic marine U-cycle box modeling (Lau et al., 2016). Similarly to the C-P-U model, this forward model also allows the quantitative evaluation of the redox changes in the ocean. However, it does not link the changes of the U-cycle to those of other geochemical cycles (e.g. C, P), hence it cannot give direct insight into the causes of anoxia and its relation to the LIP pulses. The initial, perturbing parameter is an assumed change in the extent of seafloor anoxia, and the altered uranium fluxes and related isotopic fractionation are modeled under non-steady-state conditions (Supplementary material). Overall, the U-cycle box model shows a similar trend compared to the C-P-U model indicating a prolonged anoxic event in the Hettangian with the most severe anoxic conditions (∼11%) reached 210–260 kyr af-

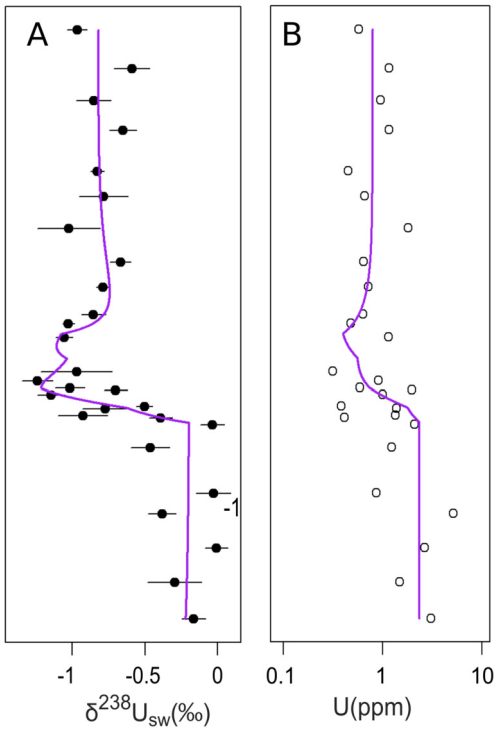

Fig. 5. (A) The uranium isotope and (B) uranium concentration data of Csővár overlain with the results of U-cycle box modeling (purple curves).

ter the main extinction phase (Fig. 5, Fig. 4D, Table S2). However, it estimates more anoxia for the first 100 kyr of the environmental perturbation. Note that there is a lag between the onset of the measured and the C-P-U modeled uranium isotope anomaly (Fig. 4F). Modeling the observed abrupt drop of uranium isotope values is only possible by assuming highly unrealistic volcanic C emission rates. One explanation for the observed lag involves that the C-P-U model does not account for additional anoxia-inducing mechanisms that may have been significant at the beginning of the perturbation, e.g. temperature-related water-column stratification, decreased solubility of O_2 in the ocean due to greenhouse climate, and changes in the atmospheric O_2 level (Falkowski et al., 2005).

Despite the useful insights that can be gained from the models, there are limitations to the U-cycle and C-P-U modeling. Significantly different histories of anoxia can be modeled by using the minimum, maximum, or average estimated fractionation factors (Fig. 5F, Fig. S5), riverine δ^{238}U, and initial seawater δ^{238}U. The uranium isotope ratios of the ancient ocean and rivers remain unknown, and the mechanisms controlling the fractionation factors are yet to be fully understood.

Our results are in broad agreement with the first published δ^{238}U study about the ETE (Jost et al., 2017b) which indicates extensive (40–100-fold) and prolonged bottom-water anoxia based on U-cycle box modeling results, but a duration of only 50 kyr is suggested for the anoxic event. Uncertainties in the correlation of TJB sections also affect the comparison of the model results (Fig. S5). Whilst we infer that the duration of the anoxic event was longer based on the astrochronology at Csővár, our results confirm the suggestion that marine anoxia developed at the end of the Triassic and continued until the Hettangian (Jost et al., 2017b).

There are relatively few observations available about the redox conditions during the later part of Hettangian, but the majority of them support our findings. Data from different European epicontinental locations indicate that anoxia persisted from the middle Hettangian until the early Sinemurian (Luo et al., 2018; Richoz et al., 2012) but other observations from Panthalassa suggest mainly oxic conditions (Fujisaki et al., 2016; Wignall et al., 2010) except for one study (Kasprak et al., 2015). The deposition of organic-rich mudrocks during the early Hettangian was widespread in the well-studied sections of the northwest European epicontinental sea (van de Schootbrugge et al., 2013). Our results are only in partial agreement with the suggestion of two phases of anoxia for the ETE, the first one being short and intense and the second one is longer and more widespread, with a long, relatively oxygenated interval between them (Wignall and Atkinson, 2020). The model estimates of the extent of anoxic seafloor are lower than those for the end-Permian extinction (>18%, Zhang et al., 2020), but comparable to the estimates for the mid-Cretaceous Oceanic Anoxic Event 2 (8-15%, Clarkson et al., 2018).

5.4. Causes of persistent anoxia and its effect on biotic recovery

After the ETE, mass mortality may have exacerbated oxygen depletion as large amounts of degrading organic matter consumed the dissolved oxygen in seawater. However, enhanced marine organic matter burial, resulting from high productivity and increased burial in anoxic sediments, act as a sink for CO_2, and sequestration of this greenhouse gas induces a negative feedback loop that would lead to decreasing temperatures and weathering intensity, and consequently, decreasing anoxia. Counteracting this effect, the repeated pulses of CAMP eruptions injected excess CO_2 into the atmosphere, thereby sustaining the biogeochemical perturbations and preventing the rebound from anoxia. The interval of the most severe anoxia (13%, Fig. 4D) 200–250 kyr after the onset of the perturbations was likely the consequence of the initial extrusive CAMP phase marked by the most prominent Hg peaks of the section (Fig. 1, Fig. 4A). The prolonged CAMP activity and concomitant CO_2 degassing are thought to sustain the protracted anoxia, as indicated by both the very low δ^{238}U values (average of −0.84‰, Fig. 1) and the modeled high anoxic seafloor extent (1–6%, Fig. 4D) throughout the early to middle Hettangian. Indeed, for the benthic fauna, it took much longer to recover after the biotic crisis than for the nektonic fauna (Damborenea et al., 2017; Wignall and Atkinson, 2020). Thus the bottom-water anoxia probably played an important role in delaying the biotic recovery after the ETE.

6. Conclusions

A new uranium isotope dataset from the TJB section of Csővár shows a major negative anomaly. We employed Earth system modeling to estimate the changes in parameters that may drive this anomaly, especially to understand the role of anoxia in driving the extinction and/or delaying the subsequent biotic recovery. Although the low Mn/Sr ratios and other geochemical evidence indicate only limited diagenetic alteration, the U concentrations are higher than expected for the primary calcite mineralogy and may suggest some authigenic U incorporation.

The low TOC, whole-rock V, and Mn content reflect the oxic depositional environment in the Csővár basin. The presence of a negative Ce anomaly within the boundary interval suggests well-oxygenated bottom-water conditions in the Csővár basin during the global perturbation events. Hence, in the lack of indication of local hypoxia, we infer that δ^{238}U values are representative of the world ocean. The position of the negative uranium isotope anomaly and the trends of the δ^{238}U curve are similar to those of the Lombardian TJB sections confirming that the δ^{238}U signal of the Csővár section is a global phenomenon.

Comparison of the uranium isotope data from the Csővár section with the only previously published δ^{238}U record across the TJB is hampered by uncertainties of correlation. Nevertheless, the uranium isotope trends of the three sections are similar, but the dif-

ferent magnitudes of the $\delta^{238}U$ excursions observed in the Csővár and the Lombardian sections warrant further study.

The abrupt and major $\delta^{238}U$ decline from −0.39‰ to −0.93‰ before the TJB suggests a rapid increase in the global extent of bottom-water anoxia and confirms the observations and findings of the previous $\delta^{238}U$ study across the TJB. This anomaly coincides with the previously detected carbon isotope anomaly (ICIE) which is associated with the first, major intrusive phase of the CAMP activity and marks the extinction horizon (ETE). Our results support the hypothesis that volcanism indirectly induced anoxia in the ocean.

Results of the C-P-U and the dynamic uranium box modeling indicate that anoxia did not reach its maximum extent during the extinction but only 200–250 kyr later, when approximately 13% of the global ocean floor may have been anoxic. The extent of seafloor anoxia likely remained high (1–6%) throughout most of the Hettangian. The severity of anoxia during the extinction event might be slightly underestimated as certain potentially anoxia-inducing mechanisms are not included in the models.

The delayed peak of anoxia is probably the result of the later, extrusive phase of the CAMP that is marked by the prominent Hg peak of the section. The subsequent minor Hg peaks and NCIEs recorded in the upper part of the section indicate further volcanic pulses in the Hettangian. Our data and modeling results confirm that the prolonged CAMP activity and related CO_2 degassing are probably responsible for the persistent anoxia. The existence of anoxia in the middle Hettangian explains the slow rebound of benthic fauna after the extinction. Our findings indicate that the spread of anoxia and the ETE have a common cause rather than a direct cause-and-effect relationship, but prolonged bottom-water anoxia delayed the biotic recovery after the extinction.

CRediT authorship contribution statement

Anna Somlyay: Investigation, Visualization, Writing – original draft, Review & editing. **László Palcsu**: Methodology, Investigation, Writing – review and editing. **Gabriella Kiss**: Methodology, Investigation, Writing – review and editing. **Matthew Clarkson**: Methodology, Investigation, Writing – review and editing. **Emma Blanka Kovács**: Sample collection, Writing – review & editing. **Zsolt Vallner**: Investigation, Writing – review & editing. **Norbert Zajzon**: Sample collection, Investigation, Writing – review & editing. **József Pálfy**: Conceptualization, Sample collection, Writing – original draft, review & editing.

Declaration of competing interest

The authors declare that they have no known competing financial interests or personal relationships that could have appeared to influence the work reported in this paper.

Data availability

All data are included in the Supplementary material.

Acknowledgements

We are grateful to Steve Romaniello for his suggestions regarding the analytical procedure and Mihály Braun for the elemental concentration measurements. Zsófia Kovács is thanked for help in sample collection for REE analyses. We thank János Haas for the helpful comments. Constructive reviews by three anonymous reviewers helped improve the manuscript. Funding from NKFIH OTKA Grant K135309 is acknowledged. The research was partly supported by the European Union and the State of Hungary, co-financed by the European Regional Development Fund in the project of GINOP-2.3.2.-15-2016-00009 'ICER'. This is ELKH-MTM-ELTE Paleo contribution No. 370.

Appendix A. Supplementary material

Supplementary material related to this article can be found online at https://doi.org/10.1016/j.epsl.2023.118190.

References

Andersen, M.B., Romaniello, S., Vance, D., Little, S.H., Herdman, R., Lyons, T.W., 2014. A modern framework for the interpretation of $^{238}U/^{235}U$ in studies of ancient ocean redox. Earth Planet. Sci. Lett. 400, 184–194. https://doi.org/10.1016/j.epsl.2014.05.051.

Andersen, M.B., Stirling, C.H., Weyer, S., 2017. Uranium isotope fractionation. Rev. Mineral. Geochem. 82 (1), 799–850. https://doi.org/10.2138/rmg.2017.82.19.

Bachan, A., Payne, J.L., 2015. Modelling the impact of pulsed CAMP volcanism on pCO_2 and $\delta^{13}C$ across the Triassic–Jurassic transition. Geol. Mag. 153, 252–270. https://doi.org/10.1017/S0016756815000126.

Bartlett, R., Elrick, M., Wheeley, J.R., Polyak, V., Desrochers, A., Asmerom, Y., 2018. Abrupt global-ocean anoxia during the Late Ordovician–Early Silurian detected using uranium isotopes of marine carbonates. Proc. Natl. Acad. Sci. USA 115 (23), 5896–5901. https://doi.org/10.1073/pnas.1802438115.

Brand, U., 2004. Carbon, oxygen and strontium isotopes in Paleozoic carbonate components: an evaluation of original seawater-chemistry proxies. Chem. Geol. 204, 23–44. https://doi.org/10.1016/j.chemgeo.2003.10.013.

Brennecka, G.A., Borg, L.E., Hutcheon, I.D., Sharp, M.A., Anbar, A.D., 2010. Natural variations in uranium isotope ratios of uranium ore concentrates: understanding the $^{238}U/^{235}U$ fractionation mechanism. Earth Planet. Sci. Lett. 291 (1–4), 228–233. https://doi.org/10.1016/j.epsl.2010.01.023.

Chen, X., Romaniello, S.J., Herrmann, A.D., Wasylenki, L.E., Anbar, A.D., 2016. Uranium isotope fractionation during coprecipitation with aragonite and calcite. Geochim. Cosmochim. Acta 188, 189–207. https://doi.org/10.1016/j.gca.2016.05.022.

Chen, X., Romaniello, S.J., Anbar, A.D., 2017. Uranium isotope fractionation induced by aqueous speciation: implications for U isotopes in marine $CaCO_3$ as a paleoredox proxy. Geochim. Cosmochim. Acta 215, 162–172. https://doi.org/10.1016/j.gca.2017.08.006.

Chen, X., Romaniello, S.J., Herrmann, A.D., Hardisty, D., Gill, B.C., Anbar, A.D., 2018a. Diagenetic effects on uranium isotope fractionation in carbonate sediments from the Bahamas. Geochim. Cosmochim. Acta 237, 294–311. https://doi.org/10.1016/j.gca.2018.06.026.

Chen, X., Romaniello, S.J., Herrmann, A.D., Samankassou, E., Anbar, A.D., 2018b. Biological effects on uranium isotope fractionation ($^{238}U/^{235}U$) in primary biogenic carbonates. Geochim. Cosmochim. Acta 240, 1–10. https://doi.org/10.1016/j.gca.2018.08.028.

Chen, X., Romaniello, S.J., McCormick, M., Sherry, A., Havig, J.R., Zheng, W., Anbar, A.D., 2021. Anoxic depositional overprinting of $^{238}U/^{235}U$ in calcite: when do carbonates tell black shale tales? Geology 49 (10), 1193–1197. https://doi.org/10.1130/g48949.1.

Chen, X., Robinson, S.A., Romaniello, S.J., Anbar, A.D., 2022. $^{238}U/^{235}U$ in calcite is more susceptible to carbonate diagenesis. Geochim. Cosmochim. Acta 326, 273–287. https://doi.org/10.1016/j.gca.2022.03.027.

Clarkson, M.O., Stirling, C.H., Jenkyns, H.C., Dickson, A.J., Porcelli, D., Moy, C.M., Pogge von Strandmann, P.A.E., Cooke, I.R., Lenton, T.M., 2018. Uranium isotope evidence for two episodes of deoxygenation during Oceanic Anoxic Event 2. Proc. Natl. Acad. Sci. USA 115, 2918–2923. https://doi.org/10.1073/pnas.1715278115.

Clarkson, M.O., Hennekam, R., Sweere, T.C., Andersen, M.B., Reichart, G.-J., Vance, D., 2021. Carbonate associated uranium isotopes as a novel local redox indicator in oxidatively disturbed reducing sediments. Geochim. Cosmochim. Acta 311, 12–28. https://doi.org/10.1016/j.gca.2021.07.025.

Cohen, A.S., Coe, A.L., 2007. The impact of the Central Atlantic Magmatic Province on climate and on the Sr- and Os-isotope evolution of seawater. Palaeogeogr. Palaeoclimatol. Palaeoecol. 244, 374–390. https://doi.org/10.1016/j.palaeo.2006.06.036.

Damborenea, S.E., Echevarría, J., Ros-Franch, S., 2017. Biotic recovery after the end-Triassic extinction event: evidence from marine bivalves of the Neuquén Basin, Argentina. Palaeogeogr. Palaeoclimatol. Palaeoecol. 487, 93–104. https://doi.org/10.1016/j.palaeo.2017.08.025.

Davies, J.H.F.L., Marzoli, A., Bertrand, H., Youbi, N., Ernesto, M., Schaltegger, U., 2017. End-Triassic mass extinction started by intrusive CAMP activity. Nat. Commun. 8, 15596. https://doi.org/10.1038/ncomms15596.

Dunk, R.M., Mills, R.A., Jenkins, W.J., 2002. A reevaluation of the oceanic uranium budget for the Holocene. Chem. Geol. 190, 45–67. https://doi.org/10.1016/S0009-2541(02)00110-9.

Falkowski, P.G., Katz, M.E., Milligan, A.J., Fennel, K., Cramer, B.S., Aubry, M.P., Berner, R.A., Novacek, M.J., Zapol, W.M., 2005. The rise of oxygen over the past 205 million years and the evolution of large placental mammals. Science 309, 2202–2204. https://doi.org/10.1126/science.1116047.

Fujisaki, W., Sawaki, Y., Yamamoto, S., Sato, T., Nishizawa, M., Windley, B.F., Maruyama, S., 2016. Tracking the redox history and nitrogen cycle in the pelagic Panthalassic deep ocean in the Middle Triassic to Early Jurassic: insights from redox-sensitive elements and nitrogen isotopes. Palaeogeogr. Palaeoclimatol. Palaeoecol. 449, 397–420. https://doi.org/10.1016/j.palaeo.2016.01.039.

Gaetani, M., 1970. Faune Hettangiane della parte Orientale della provincia di Bergamo. Riv. Ital. Paleontol. 76, 355–442.

Galli, M.T., Jadoul, F., Bernasconi, S.M., Weissert, H., 2005. Anomalies in global carbon cycling and extinction at the Triassic/Jurassic boundary: evidence from a marine C-isotope record. Palaeogeogr. Palaeoclimatol. Palaeoecol. 216 (3–4), 203–214. https://doi.org/10.1016/j.palaeo.2004.11.009.

Galli, M.T., Jadoul, F., Bernasconi, S.M., Cirilli, S., Weissert, H., 2007. Stratigraphy and palaeoenvironmental analysis of the Triassic-Jurassic transition in the western Southern Alps (Northern Italy). Palaeogeogr. Palaeoclimatol. Palaeoecol. 244, 52–70. https://doi.org/10.1016/j.palaeo.2006.06.023.

Greene, S.E., Martindale, R.C., Ritterbush, K.A., Bottjer, D.J., Corsetti, F.A., Berelson, W.M., 2012. Recognising ocean acidification in deep time: an evaluation of the evidence for acidification across the Triassic-Jurassic boundary. Earth-Sci. Rev. 113, 72–93. https://doi.org/10.1016/j.earscirev.2012.03.009.

Haas, J., Götz, A.E., Pálfy, J., 2010. Late Triassic to Early Jurassic palaeogeography and eustatic history in the NW Tethyan realm: new insights from sedimentary and organic facies of the Csovar Basin (Hungary). Palaeogeogr. Palaeoclimatol. Palaeoecol. 291, 456–468. https://doi.org/10.1016/j.palaeo.2010.03.014.

Haas, J., Tardy-Filácz, E., 2004. Facies changes in the Triassic-Jurassic boundary interval in an intraplatform basin succession at Csovar (Transdanubian Range, Hungary). Sediment. Geol. 168, 19–48. https://doi.org/10.1016/j.sedgeo.2004.03.002.

Hallam, A., 1995. Oxygen-restricted facies of the basal Jurassic of northwest Europe. Hist. Biol. 10, 247–257. https://doi.org/10.1080/10292389509380523.

He, T., Corso, J., Newton, R., Wignall, P., Mills, B., Todaro, S., Stefano, P., Turner, E., Jamieson, R., Randazzo, V., Rigo, M., Jones, R., Dunhill, A., 2020. An enormous sulfur isotope excursion indicates marine anoxia during the end-Triassic mass extinction. Sci. Adv. 6, eabb6704. https://doi.org/10.1126/sciadv.abb6704.

Heimdal, T.H., Jones, M.T., Svensen, H.H., 2020. Thermogenic carbon release from the Central Atlantic magmatic province caused major end-Triassic carbon cycle perturbations. Proc. Natl. Acad. Sci. USA, 202000095. https://doi.org/10.1073/pnas.2000095117.

Hesselbo, S.P., Robinson, S.A., Surlyk, F., Piasecki, S., 2002. Terrestrial and marine mass extinction at the Triassic–Jurassic boundary synchronized with major carbon-cycle perturbation: a link to initiation of massive volcanism? Geology 30, 251–254. https://doi.org/10.1130/0091-7613(2002)030<0251:TAMEAT>2.0.CO;2.

Hood, A.v.S., Planavsky, N.J., Wallace, M.W., Wang, X., Bellefroid, E.J., Gueguen, B., Cole, D.B., 2016. Integrated geochemical-petrographic insights from component-selective δ^{238}U of Cryogenian marine carbonates. Geology 44 (11), 935–938. https://doi.org/10.1130/g38533.1.

Jadoul, F., Galli, M.T., 2008. The Hettangian shallow water carbonates after the Triassic/Jurassic biocalcification crisis: the Albenza Formation in the western Southern Alps. Riv. Ital. Paleontol. Stratigr. 114, 453–470.

Jost, A.B., Bachan, A., van de Schootbrugge, B., Brown, S.T., DePaolo, D.J., Payne, J.L., 2017a. Additive effects of acidification and mineralogy on calcium isotopes in Triassic/Jurassic boundary limestones. Geochem. Geophys. Geosyst. 18 (1), 113–124. https://doi.org/10.1002/2016gc006724.

Jost, A.B., Bachan, A., van de Schootbrugge, B., Lau, K.V., Weaver, K.L., Maher, K., Payne, J.L., 2017b. Uranium isotope evidence for an expansion of marine anoxia during the end-Triassic extinction. Geochem. Geophys. Geosyst. 1 (16). https://doi.org/10.1002/2017GC006941.

Kasprak, A.H., Sepúlveda, J., Price-Waldman, R., Williford, K.H., Schoepfer, S.D., Haggart, J.W., Ward, P.D., Summons, R.E., Whiteside, J.H., 2015. Episodic photic zone euxinia in the northeastern Panthalassic Ocean during the end-Triassic extinction. Geology 43 (4), 307–310. https://doi.org/10.1130/g36371.1.

Kiessling, W., Simpson, C., Foote, M., 2010. Reefs as cradles of evolution and sources of biodiversity in the Phanerozoic. Science 327, 196–198. https://doi.org/10.1126/science.1182241.

Korte, C., Ruhl, M., Pálfy, J., Ullmann, C.V., Hesselbo, S.P., 2019. Chemostratigraphy across the Triassic–Jurassic boundary. In: Sial, A.N., Gaucher, C., Ramkumar, M., Ferreira, V.P. (Eds.), Chemostratigraphy Across Major Chronological Boundaries, pp. 185–210.

Kovács, E.B., Ruhl, M., Demény, A., Fórizs, I., Hegyi, I., Horváth-Kostka, Z.R., Móricz, F., Vallner, Z., Pálfy, J., 2020. Mercury anomalies and carbon isotope excursions in the western Tethyan Csővár section support the link between CAMP volcanism and the end-Triassic extinction. Glob. Planet. Change 194, 103291. https://doi.org/10.1016/j.gloplacha.2020.103291.

Lau, K.V., Maher, K., Altiner, D., Kelley, B.M., Kump, L.R., Lehrmann, D.J., Silva-Tamayo, J.C., Weaver, K.L., Yu, M., Payne, J.L., 2016. Marine anoxia and delayed Earth system recovery after the end-Permian extinction. Proc. Natl. Acad. Sci. USA 113, 2360–2365. https://doi.org/10.1073/pnas.1515080113.

Lenton, T.M., Daines, S.J., Mills, B.J.W., 2018. COPSE reloaded: an improved model of biogeochemical cycling over Phanerozoic time. Earth-Sci. Rev. 178, 1–28. https://doi.org/10.1016/j.earscirev.2017.12.004.

Lindström, S., Sanei, H., van de Schootbrugge, B., Pedersen, G.K., Lesher, C.E., Tegner, C., Heunisch, C., Dybkjær, K., Outridge, P.M., 2019. Volcanic Mercury and mutagenesis in land plants during the end-Triassic mass extinction. Sci. Adv. 5 (10). https://doi.org/10.1126/sciadv.aaw4018.

Livermore, B.D., Dahl, T.W., Bizzarro, M., Connelly, J.N., 2020. Uranium isotope compositions of biogenic carbonates - Implications for U uptake in shells and the application of the paleo-ocean oxygenation proxy. Geochim. Cosmochim. Acta 287, 50–64. https://doi.org/10.1016/j.gca.2020.07.005.

Luo, G., Richoz, S., van de Schootbrugge, B., Algeo, T.J., Xie, S., Ono, S., Summons, R.E., 2018. Multiple sulfur-isotopic evidence for a shallowly stratified ocean following the Triassic-Jurassic boundary mass extinction. Geochim. Cosmochim. Acta 231, 73–87. https://doi.org/10.1016/j.gca.2018.04.015.

Marzoli, A., Bertrand, H., Knight, K.B., Cirilli, S., Buratti, N., Verati, C., Nomade, S., Renne, P.R., Youbi, N., Martini, R., Allenbach, K., Neuwerth, R., Rapaille, C., Zaninetti, L., Bellieni, G., 2004. Synchrony of the Central Atlantic magmatic province and the Triassic-Jurassic boundary climatic and biotic crisis. Geology 32, 973–976. https://doi.org/10.1130/G20652.1.

Marzoli, A., Bertrand, H., Youbi, N., Callegaro, S., Merle, R., Reisberg, L., Chiaradia, M., Brownlee, S., Jourdan, F., Zanetti, A., Davies, J., Cuppone, T., Mahmoudi, A., Medina, F., Renne, P.R., Bellieni, G., Crivellari, S., El Hachimi, H., Bensalah, M.K., Meyzen, C.M., Tegner, C., 2019. The Central Atlantic magmatic province (CAMP) in Morocco. J. Petrol. 60 (5), 945–996. https://doi.org/10.1093/petrology/egz021.

McElwain, J.C., Beerling, D.J., Woodward, F.I., 1999. Fossil plants and global warming at the Triassic-Jurassic boundary. Science 285, 1386–1390. https://doi.org/10.1126/science.285.5432.1386.

Muttoni, G., Kent, D.V., Jadoul, F., Olsen, P.E., Rigo, M., Galli, M.T., Nicora, A., 2010. Rhaetian magneto-biostratigraphy from the Southern Alps (Italy): constraints on Triassic chronology. Palaeogeogr. Palaeoclimatol. Palaeoecol. 285, 1–16. https://doi.org/10.1016/j.palaeo.2009.10.014.

Noordmann, J., Weyer, S., Montoya-Pino, C., Dellwig, O., Neubert, N., Eckert, S., Paetzel, M., Böttcher, M.E., 2015. Uranium and molybdenum isotope systematics in modern euxinic basins: case studies from the Central Baltic Sea and the Kyllaren Fjord (Norway). Chem. Geol. 396, 182–195. https://doi.org/10.1016/j.chemgeo.2014.12.012.

Pálfy, J., Demény, A., Haas, J., Carter, E.S., Görög, Á., Halász, D., Oravecz-Scheffer, A., Hetényi, M., Márton, E., Orchard, M.J., Ozsvárt, P., Vető, I., Zajzon, N., 2007. Triassic-Jurassic boundary events inferred from integrated stratigraphy of the Csővár section, Hungary. Palaeogeogr. Palaeoclimatol. Palaeoecol. 244, 11–33. https://doi.org/10.1016/j.palaeo.2006.06.021.

Pálfy, J., Demény, A., Haas, J., Hetényi, M., Orchard, M., Vető, I., 2001. Carbon isotope anomaly and other geochemical changes at the Triassic-Jurassic boundary from a marine section in Hungary. Geology 29, 1047–1050. https://doi.org/10.1130/0091-7613(2001)029<1047:CIAAOG>2.0.CO;2.

Percival, L.M.E., Ruhl, M., Hesselbo, S.P., Jenkyns, H.C., Mather, T.A., Whiteside, J.H., 2017. Mercury evidence for pulsed volcanism during the end-Triassic mass extinction. Proc. Natl. Acad. Sci. USA 114, 7929–7934. https://doi.org/10.1073/pnas.1705378114.

Richoz, S., van de Schootbrugge, B., Pross, J., Puttmann, W., Quan, T.M., Lindstrom, S., Heunisch, C., Fiebig, J., Maquil, R., Schouten, S., Hauzenberger, C.A., Wignall, P.B., 2012. Hydrogen sulphide poisoning of shallow seas following the end-Triassic extinction. Nat. Geosci. 5, 662–667. https://doi.org/10.1038/ngeo1539.

Romaniello, S.J., Herrmann, A.D., Anbar, A.D., 2013. Uranium concentrations and ^{238}U/^{235}U isotope ratios in modern carbonates from the Bahamas: Assessing a novel paleoredox proxy. Chem. Geol. 362, 305–316. https://doi.org/10.1016/j.chemgeo.2013.10.002.

Rolison, J.M., Stirling, C.H., Middag, R., Rijkenberg, M.J.A., 2017. Uranium stable isotope fractionation in the Black Sea: Modern calibration of the ^{238}U/^{235}U paleoredox proxy. Geochim. Cosmochim Acta 203, 69–88. https://doi.org/10.1016/j.gca.2016.12.013.

Ruhl, M., Kuerschner, W.M., Krystyn, L., 2009. Triassic-Jurassic organic carbon isotope stratigraphy of key sections in the western Tethys realm (Austria). Earth Planet. Sci. Lett. 281, 169–187. https://doi.org/10.1016/j.epsl.2009.02.020.

Ruhl, M., Hesselbo, S.P., Al-Suwaidi, A., Jenkyns, H.C., Damborenea, S.E., Manceñido, M.O., Storm, M., Mather, T.A., Riccardi, A.C., 2020. On the onset of Central Atlantic Magmatic Province (CAMP) volcanism and environmental and carbon-cycle change at the Triassic–Jurassic transition (Neuquén Basin, Argentina). Earth-Sci. Rev. 208, 103229. https://doi.org/10.1016/j.earscirev.2020.103229.

Schaller, M.F., Wright, J.D., Kent, D.V., 2011. Atmospheric pCO_2 perturbations associated with the Central Atlantic Magmatic Province. Science 331, 1404–1409. https://doi.org/10.1126/science.1199011.

Schoene, B., Guex, J., Bartolini, A., Schaltegger, U., Blackburn, T.J., 2010. Correlating the end-Triassic mass extinction and flood basalt volcanism at the 100 ka level. Geology 38 (5), 387–390. https://doi.org/10.1130/g30683.1.

Sepkoski Jr., J.J., 1996. Patterns of Phanerozoic extinction: a perspective from global data bases. In: Walliser, O.H. (Ed.), Global Events and Event Stratigraphy in the Phanerozoic. Springer, Berlin, pp. 35–51.

Sholkovitz, E.R., Landing, W.M., Lewis, B.L., 1994. Ocean particle chemistry: The fractionation of rare earth elements between suspended particles and seawater. Geochimica et Cosmochimica Acta 58 (7), 1567–1579. https://doi.org/10.1016/0016-7037(94)90549-7.

Thibodeau, A.M., Ritterbush, K., Yager, J.A., West, A.J., Ibarra, Y., Bottjer, D.J., Berelson, W.M., Bergquist, B.A., Corsetti, F.A., 2016. Mercury anomalies and the timing of

biotic recovery following the end-Triassic mass extinction. Nat. Commun. 7 (1). https://doi.org/10.1038/ncomms11147.

Tostevin, R., 2021. Cerium Anomalies and Paleoredox. Cambridge University Press, Cambridge.

Tissot, F.L.H., Dauphas, N., 2015. Uranium isotopic compositions of the crust and ocean: Age corrections, U budget and global extent of modern anoxia. Geochimica et Cosmochimica Acta 167, 113–143. https://doi.org/10.1016/j.gca.2015.06.034.

Tissot, F.L.H., Chen, C., Go, B.M., Naziemiec, M., Healy, G., Bekker, A., Swart, P.K., Dauphas, N., 2018. Controls of eustasy and diagenesis on the $^{238}U/^{235}U$ of carbonates and evolution of the seawater ($^{234}U/^{238}U$) during the last 1.4 Myr. Geochim. Cosmochim. Acta 242, 233–265. https://doi.org/10.1016/j.gca.2018.08.022.

Vallner, Z., Kovács, E.B., Haas, J., Móricz, F., Ruhl, M., Zajzon, N., Pálfy, J., 2023. Preservation of orbital forcing in intraplatform carbonates and an astronomical time frame for a multiproxy record of end-Triassic global change from a western Tethyan section (Csővár, Hungary). Palaeogeogr. Palaeoclimatol. Palaeoecol. 111493. https://doi.org/10.1016/j.palaeo.2023.111493.

van de Schootbrugge, B., Bachan, A., Suan, G., Richoz, S., Payne, J.L., 2013. Microbes, mud and methane: cause and consequence of recurrent Early Jurassic anoxia following the end-Triassic mass extinction. Palaeontology 56, 685–709. https://doi.org/10.1111/pala.12034.

van de Schootbrugge, B., Payne, J.L., Tomasovych, A., Pross, J., Fiebig, J., Benbrahim, M., Follmi, K.B., Quan, T.M., 2008. Carbon cycle perturbation and stabilization in the wake of the Triassic-Jurassic boundary mass-extinction event. Geochem. Geophys. Geosyst. 9, 1–16. https://doi.org/10.1029/2007GC001914.

Ward, P.D., Haggart, J.W., Carter, E.S., Wilbur, D., Tipper, H.W., Evans, T., 2001. Sudden productivity collapse associated with the Triassic-Jurassic boundary mass extinction. Science 292 (5519), 1148–1151. https://doi.org/10.1126/science.1058574.

Weyer, S., Anbar, A.D., Gerdes, A., Gordon, G.W., Algeo, T.J., Boyle, E.A., 2008. Natural fractionation of $^{238}U/^{235}U$. Geochim. Cosmochim. Acta 72, 345–359. https://doi.org/10.1016/j.gca.2007.11.012.

Wignall, P.B., Atkinson, J.W., 2020. A two-phased end-Triassic mass extinction. Earth-Sci. Rev. 103282. https://doi.org/10.1016/j.earscirev.2020.103282.

Wignall, P.B., Bond, D.P.G., Kuwahara, K., Kakuwa, Y., Newton, R.J., Poulton, S.W., 2010. An 80 million year oceanic redox history from Permian to Jurassic pelagic sediments of the Mino-Tamba terrane, SW Japan, and the origin of four mass extinctions. Glob. Planet. Change 71, 109–123. https://doi.org/10.1016/j.gloplacha.2010.01.022.

Zhang, F., Algeo, T.J., Romaniello, S.J., Cui, Y., Zhao, L., Chen, Z.-Q., Anbar, A.D., 2018. Congruent Permian-Triassic $\delta^{238}U$ records at Panthalassic and Tethyan sites: confirmation of global-oceanic anoxia and validation of the U-isotope paleoredox proxy. Geology 46, 327–330. https://doi.org/10.1130/G39695.1.

Zhang, F., Shen, S.-z., Cui, Y., Lenton, T.M., Dahl, T.W., Zhang, H., Zheng, Q.-f., Wang, W., Krainer, K., Anbar, A.D., 2020. Two distinct episodes of marine anoxia during the Permian-Triassic crisis evidenced by uranium isotopes in marine dolostones. Geochim. Cosmochim. Acta 287, 165–179. https://doi.org/10.1016/j.gca.2020.01.032.